Following Zn corrosion during long term immersion test in physiological solutions to establish the potential of zinc as biodegradable prosthetic material

ChemSusChem

Research Article
doi.org/10.1002/cssc.202401546

Chemistry Europe
European Chemical Societies Publishing

www.chemsuschem.org

Unraveling the Role of CuO in Cu_xO/TiO_2 Photocatalyst for the Direct Propylene Epoxidation With O_2 in a Fluidized Bed Reactor

Nicola Morante,[a] Olimpia Tammaro,[b] Katia Monzillo,[a] Diana Sannino,[a] Alfio Battiato,[c] Ettore Vittone,[c] Micaela Castellino,[b, d] Serena Esposito,*[b] and Vincenzo Vaiano*[a]

Propylene epoxidation in mild conditions using molecular O_2 is a highly desirable reaction that represents a significant challenge in the field of heterogeneous catalysis for the synthesis of oxygenated organic compounds of industrial interest. In this work, Cu_xO/TiO_2 composites with different mominal CuO loadings (in the range of 0.5–8.4 wt%) were used to promote the photocatalytic epoxidation of propylene with molecular oxygen under UV-A irradiation in a fluidized bed system. The photocatalysts were prepared by a straightforward method consisting of thermal annealing of physical mixtures between copper acetate and sol-gel-derived TiO_2. Different characterization techniques were employed to assess the influence of Cu_xO content on the physical-chemical properties of the Cu_xO/TiO_2 composites. The best combination in terms of propylene conversion and selectivity towards propylene oxide (18.1% and 72%, respectively) was obtained with Cu_xO/TiO_2 at 1.1 wt % CuO, as shown by photocatalytic tests. The high propylene oxide selectivity is due to the ability of CuO in the Cu_xO/TiO_2 composite to transform molecular O_2 into hydrogen peroxide that, in turn, is able to directly oxidize propylene to propylene oxide. By using a UV-A light intensity of 297.2 mW cm^{-2}, the propylene conversion and the epoxide yield were 31.5 and 22.2%, respectively, significantly higher than that reported in the literature. Moreover, the energy consumption of the reaction system employed in this paper was significantly lower than that of photocatalytic systems studied in the literature dealing with selective propylene epoxidation.

1. Introduction

Propylene oxide, also known as propene oxide, methyloxyrane or 1,2-epoxypropane, is an important raw material used in the chemical industry for the synthesis of several compounds, such as polyols, propylene glycol, glycol ethers, and non-ionic surfactants.[1] In particular, propylene oxide appears to be the third propylene derivative most synthesized by the process industry, following polypropylene and acetonitrile.[2–3] For this reason, the global propylene oxide market is expected to experience significant growth in the next years.

Nowadays, the synthesis of propylene oxide (PO) by industrial chemical plants occurs through five different conventional processes (Figure S1): i) Chlorohydrin Process (CL), ii) Tert-butyl alcohol co-product process (PO/TBA), iii) Styrene co-product process (PO/SM), iv) Hydrogen Peroxide Process (HPPO), and v) Cumene Process (POC).[6]

The predominant method for producing PO is the chlorohydrin procedure (CHPO), constituting 37% of global production.[6] However, to eliminate the use of chlorine in synthesis, alternative processes have been developed employing organic hydroperoxides for olefin epoxidation. Specifically, organic intermediates such as Ethylbenzene (PO/SM), isobutene (PO/TBA), or cumene (CHP) are utilized. These methods involve initial peroxidation of the intermediate molecule followed by propylene epoxidation through olefin interaction with the generated peroxide. The cumene process (CHP) offers the advantage that the coproduct, dimethylphenylmethanol, can be recycled by hydrogenation and dehydration back into cumene. On the other hand, the direct epoxidization of propylene using H_2O_2 and TS-1 catalyst,[9] with over 90% PO selectivity, commercialized by Evonik (formerly Degussa) in 2008, generates only water as a byproduct. However, the relatively high cost of H_2O_2 in 2019 (around 500 USD/t) compared to propylene oxide (PO) (approximately 1500 USD/t) poses a significant economic challenge for this process.[10] Consequently, while the preference is for oxidation using abundant and inexpensive oxygen, a catalytic process capable of selectively epoxidizing propylene remains a challenge. Indeed, the main limitation of such processes is that they do not allow direct oxidation of the olefin by molecular oxygen. This peculiarity implies the following disadvantages: i) low atom economy, ii) harsh reaction conditions (high T and P, low pH),

[a] Department of Industrial Engineering, University of Salerno, Fisciano (SA), Italy
[b] Department of Applied Science and Technology, INSTM Unit of Torino – Politecnico, Politecnico di Torino, Torino, Italy
[c] Physics Department, University of Torino, Torino, Italy
[d] Centre for Sustainable Future Technology, Istituto Italiano di Tecnologia, Torino, Italy

Correspondence: Vincenzo Vaiano, Department of Industrial Engineering, University of Salerno, Via Giovanni Paolo II 132, 84084 Fisciano (SA), Italy.
Email: vvaiano@unisa.it

Serena Esposito, Department of Applied Science and Technology, INSTM Unit of Torino – Politecnico, Politecnico di Torino, Corso Duca degli Abruzzi 24, 10129 Torino, Italy.
Email: serena_esposito@polito.it

Supporting Information for this article is available on the WWW under https://doi.org/10.1002/cssc.202401546

iii) use of toxic reactants, iv) presence of solvents and by-products, and v) complexity of the separation and purification section.[6,12]

In recent decades, research has focused on the formulation and application of thermal catalysts for the epoxidation of propylene by molecular oxygen to have a process with high epoxide yield. The best-performing catalysts in terms of conversion and selectivity are based on noble metals (silver or palladium) as active phases.[13] Although these processes have high propylene conversion values and selectivity to the desired product, they require high operating temperatures (400–500 K) and pressures (10–80 atm) and the presence of solvents (such as benzene, acetonitrile, chlorobenzene and methanol) in the reaction medium.[13]

Among the diverse array of alternative processes available, direct photocatalytic propylene epoxidation emerges as a promising and sustainable solution, exploiting molecular oxygen as an oxidant. This feasibility stems from several key factors: firstly, molecular oxygen boasts 100 wt% active oxygen, making it an ideal oxidizing agent; secondly, solar light serves as a reliable, abundant, and eco-friendly energy source; and thirdly, light-driven photo-epoxidation can be doubtless conducted in mild temperatures. Despite the numerous advantages of photo-epoxidation, practical applications encounter challenges such as inefficient utilization of light, unsatisfactory PO yield (low PO selectivity and inefficient propylene conversion), and potential photocatalyst deactivation.[15]

To navigate towards economic and environmental sustainability, the primary objective is to identify selective photocatalysts based on non-noble metals and employ a reactor configuration that enhances the performance of the reaction system.

A viable strategy involves the utilization of copper oxide-based photocatalysts, which enable in situ production of H_2O_2,[16] thereby enhancing selectivity towards the olefin epoxidation reaction.

An excellent choice for the photoreactor configuration is the use of a fluidized bed photocatalytic reactor. Indeed, this reactor configuration compared to fixed bed photoreactors shows the photoactivity increase partially associated with higher light absorption due to the utilization of scattered light by the catalysts particles and photocatalyst recirculation.[18] Furthermore, the use of a fluidized bed photoreactor enhances photonic efficiency and limits photocatalyst deactivation phenomena during oxidation reactions.[19] For these reasons, this configuration could allow a high and stable yield of propylene oxide.[23] Based on these considerations, the objective of this work was to formulate, synthesize, and test a titania-based photocatalyst with an active phase consisting of copper oxide for the selective photoepoxidation of propylene in the presence of molecular oxygen using a fluidized bed reactor. It is worthwhile to note that no scientific paper delving into the PO photocatalytic synthesis from propylene epoxidation in the presence of Cu_xO/TiO_2 composites is reported in the literature.

2. Materials and Methods

2.1. Materials

Titanium tetraisopropoxide ($C_{12}H_{28}O_4Ti$ at purity higher than 97 wt%, Sigma Aldrich), copper(II) acetate ($Cu(CO_2CH_3)_2$ at purity higher than 99 wt%, Sigma Aldrich), titanium(IV) oxysulfate solution ($TiOSO_4$ ~15% (w/w) in dilute sulfuric acid $\geq$99.99%, Sigma Aldrich), distilled water (Carlo Erba), and glass spheres (Lampugnani Sandblasting HI-TECH: 70–110 um grain size) were purchased and used as received.

2.2. Preparation of TiO_2 Used as Support for Cu_xO

The TiO_2 photocatalyst was synthesized by exploiting the advantages of the sol-gel.[24] In the preparation step, 12.5 mL of titanium tetraisopropoxide (TTIP) was added drop by drop into 25 mL of distilled water. Subsequently, the resulting mixture was stirred at room temperature for 10 min. The resulting suspension underwent centrifugation and was subjected to three washes with distilled water. Finally, the recovered materials were placed in a muffle furnace and heated to 450 °C for 30 min in a static air environment.

2.3. Preparation of Cu_xO/TiO_2 Composites

The Cu_xO/TiO_2 composites were prepared using the synthesis method proposed by Manoj et al..[26] Utilizing an agate pestle and mortar, a fixed quantity of pre-synthesized TiO_2 powder (obtained in the previous stage) underwent grinding for 3 h in conjunction with copper acetate. The resultant finely ground mixture was subjected to calcination for 1 h at 400 °C in a muffle furnace. Throughout this heating process, the combined raw materials underwent gradual decomposition and oxidation of copper acetate. Specifically, five photocatalysts at different nominal CuO loads were synthesized. The nominal percentages of copper oxide (expressed as CuO) in Cu_xO/TiO_2 composites and the amount of the copper acetate and TiO_2 employed are reported in Table S1. The photocatalysts were named CuO(x %)/TiO_2, where x% is the nominal CuO weight percentage in the photocatalysts.

2.4. Characterization of the Photocatalysts

X-ray powder diffraction (XRD) was performed on a Philips X'Pert diffractometer equipped with a Cu Kα radiation (2θ range = 20°–80°; step = 0.02° 2θ; time per step = 1 s).

The Brunauer Emmett and Teller (BET) surface area of the catalysts was assessed through dynamic N_2 adsorption measurements at −196 °C, utilizing a Costech Sorptometer 1042 following a 30 min pre-treatment in a helium flow at 150 °C. Laser Raman spectra were obtained at room temperature using a Dispersive MicroRaman (Invia, Renishaw), equipped with a 514 nm laser, covering the range of 100–800 cm^{-1} Raman shift.

The UV-A-Vis diffuse reflectance spectra (UV-A-Vis DRS) of the catalysts were acquired using a Perkin Elmer Lambda 35 spectrophotometer equipped with an RSA-PE-20 reflectance spectroscopy accessory (Labsphere Inc., North Sutton, NH). Band gap values of the nanocomposites were determined employing the Kubelka–Munk function (*KM*) and plotting $(KM \times h\nu)^2$ against $h\nu$.

A fluorescence spectrometer LS 55PerkinElmer with an Xe lamp as the excitation source was used to record the photoluminescence (PL) spectra at room temperature. The samples were excited using light of a wavelength of 362 nm.

X-ray Photoelectron Spectra on CuO(4.2%)/TiO_2 and CuO-(8.4)%/TiO_2 were acquired under ultra-high vacuum conditions (~10^{-6} Pa) using a PSP CTX400 non-monochromatic Al X-ray source (HV = 13.5 kV, emission current I_{emiss} = 12 mA) and a VSW Class 100 concentric hemispherical analyzer. A common Pass Energy (PE) value has been chosen for the survey and High Resolution (HR) spectra acquisitions, equals to 44 eV. A Cu acetate reference sample has been analysed as reference for the Cu(II) oxidation state. The analysis has been performed by means of a PHI Versaprobe 5000 with monochromatic Kα X-ray source (1486.6 eV), and a double charge compensation system, with electrons beam and Ar^+ ions. Survey and High Resolution (HR) spectra were acquired with pass energy values of 187 eV and 23 eV, respectively. Data analysis was performed with Casa XPS (Version 2.3.18) software. The calibration of the binding energy scale was achieved by assigning an energy value of 284.8 eV to the main contribution (C-C) of the C 1s region.

2.5. Photoepoxidation Activity Tests

Figure 1 depicts the schematic pictures of the experimental plant employed in this study. The experimental system comprises i) four Mass Flow Controllers (MFCs) from Brooks Instruments for precisely feeding various chemical species to the reactor (in detail C_3H_6, O_2, N_2, H_2O); ii) a temperature-controlled saturator to feed water vaporized to photoreactor; iii) the photoreactor; iv) a mass spectrometer (Trace MS; Thermo-Quest) for analyzing the composition of the gaseous stream exiting the reactor; v) a continuous CO-CO_2 analyzer (Uras 10; Hartmann & Braun).

The photoreactor used for the photocatalytic activity tests is a fluidized bed reactor. It has planar geometry, with two Pyrex windows for irradiating the photocatalytic bed, next to one of which the lighting source for activating the photocatalyst was placed. This photoreactor has already been used for photocatalytic tests for the synthesis of organic compounds through

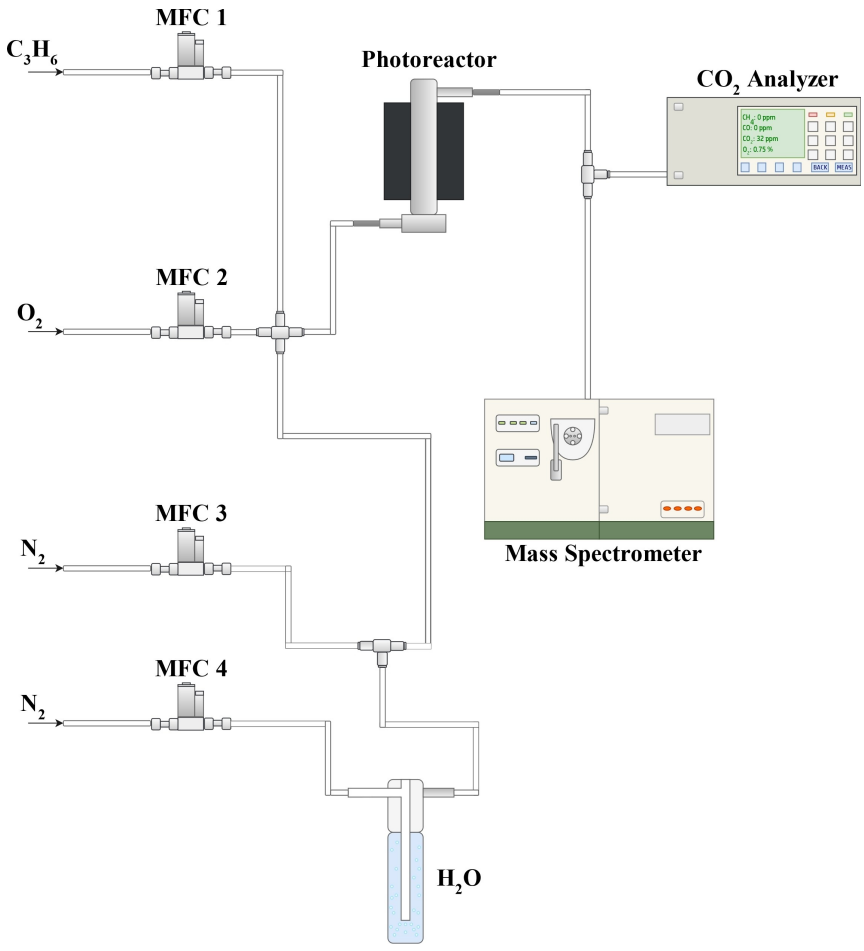

Figure 1. Schematic picture of the experimental plant used for the photoepoxidation activity tests.

selective oxidation reactions. A more complete description is reported in our previous works.[18,27] The light source is constituted by a matrix of 120 UV-A LEDs (with the wavelength emission peak centered at 365 nm) or 120 visible light LEDs (whose emission spectrum is reported in Figure S2 of Supporting Information). More details on the light sources used for the activation of the photocatalyst are reported in Supporting Information (Section SM.1).

The photocatalytic activity tests were conducted by feeding a gaseous stream consisting of C_3H_6, O_2, H_2O and N_2, with a total inlet volumetric flow rate equal to 30 L h^{-1} (STP). In particular, the inlet propylene concentration was 4000 ppm, the molar concentrations of propylene and oxygen fed into the reactor were set to the stoichiometric ratio of the olefin epoxidation reaction ($F_R = c_{C3H6}^{IN}/c_{O2}^{IN} = 2$), and the concentration of vaporized water into the inlet stream was fixed at 1000 ppm.

Before the photoepoxidation tests, a fixed quantity of photocatalyst was mixed with 20 g of glass spheres (grain size: 70–110, Lampugnani Sandblasting HI-TECH) to guarantee fluidization[23] and loaded inside the photoreactor. In particular, the experimental tests were conducted with a photocatalytic bed in a bubbling fluid regime, guaranteeing a gas surface velocity of about six times the minimum fluidization velocity. More details on the fluidization regime are given in Supporting Information (Section SM.2).

Moreover, initial tests were performed to evaluate the amount of solid particles carried out of the reactor by fluidizing the powders for several hours. No significant elutriation was observed (see section SM.3 of Supporting Information), which was also confirmed by the steady photocatalytic activity throughout the irradiation time during the photocatalytic tests (*vide infra*).

Dark equilibrium adsorption data of C_3H_6 on photocatalysts surface were obtained by integration of the concentration profiles before the photocatalytic tests. UV-A LED modules were switched on after the complete adsorption of olefin on the photocatalyst surface. All the photoepoxidation tests initially started at room temperature and when the LEDs were turned on there was an increase in temperature up to 40 °C due to the heat dissipated by the LED matrix.

The data collected by the acquisition devices were exploited to evaluate the performance of the photocatalytic reaction. The parameters analyzed were: i) the conversion of propylene (*X*), ii) the yield to PO (*Y*), iii) the selectivity to PO (*S*), and iv) the selectivity to CO and CO_2 (S_{CO+CO2}). They were calculated using the following relationships:

$$X = \left(\frac{C_{C_3H_6}^{IN} - C_{C_3H_6}^{OUT}}{C_{C_3H_6}^{IN}}\right) * 100 \quad (1)$$

$$Y = \left(\frac{C_{C_3H_6O}^{OUT}}{C_{C_3H_6}^{IN}}\right) * 100 \quad (2)$$

$$S = \left[\frac{C_{C_3H_6O}^{OUT}}{\left(C_{C_3H_6}^{IN} - C_{C_3H_6}^{OUT}\right)}\right] * 100 \quad (3)$$

$$S_{CO+CO_2} = \left[\frac{C_{CO}^{OUT} + C_{CO_2}^{OUT}}{3 * \left(C_{C_3H_6}^{IN} - C_{C_3H_6}^{OUT}\right)}\right] * 100 \quad (4)$$

Where $c_{C_3H_6}^{IN}$ is the inlet concentration of propylene, $c_{C_3H_6}^{OUT}$, $c_{C_3H_6O}^{OUT}$, c_{CO}^{OUT} and $c_{CO_2}^{OUT}$ are the outlet concentrations of propylene, propylene oxide, carbon monoxide, and carbon dioxide, respectively.

Furthermore, two experimental tests were conducted to confirm the generation of hydrogen peroxide using the optimal photocatalyst and bare TiO_2. For these tests, a gaseous feed stream with a flow rate of 30 L h^{-1} (STP) containing 1000 ppm of water, 1000 ppm of oxygen and nitrogen was fed to the reactor, and UV-A light was used to activate the photocatalytic bed. In this test, the gaseous stream exiting the reactor was conveyed into a glass bubbler containing 25 mL of distilled water. At fixed times (0 min, 15 min, 30 min, 60 min, 120 min, and 180 min), 1 mL of solution was taken, and the presence of H_2O_2 was determined by adding 300 μL of titanium(IV) oxysulfate solution to each sample and and by measuring the absorbance of the H_2O_2/$TiOSO_4$ complex at $\lambda = 410$ nm[29] using a UV-Vis spectrophotometer (Lambda 35, PerkinElmer).

3. Results and Discussion

3.1. Photocatalysts Characterization

Figure 2 shows the XRD patterns of the bare titania and the copper-loaded titania samples. As commonly observed for samples prepared by the sol-gel method and calcined at temperatures below 600 °C, titania displays the peaks of the anatase phase, although a weak 2-theta signal at around 30.8 reveals the presence of a tiny fraction of brookite, being the other peaks common to the anatase phase.[31] The formation of copper oxide can be easily recognized starting from the sample containing the lower copper content, CuO(0.5 %)/TiO_2, through the signals at 35.5° and 38.9° (CuO JCPDS card no. 00-041-0254). In particular, it is possible to observe the presence a weak peaks due to copper oxide at 38.9° for the photocatalysts at CuO content of 0.5 and 1.1 wt %, evidencing the presence of small-sized crystallites copper oxide in such samples.[34] As the copper content increases, the peaks at 35.5 and 38.9° also become more evident, confirming the formation of CuO with crystallite size greater than 4 nm[35] and proving the effectiveness of the heterojunction synthesis method. The formation of Cu_2O, if present to any extent, is hardly detectable because the most intense peak (37.105° in JCPDS card 35–1091) overlaps with one of titania anatase (JCPDS card 01-078-2486).

XPS technique was involved to shed light on the oxidation state of Cu.[36] We started looking at the reference sample of Cu acetate, to verify the Cu state of the precursor. After a survey

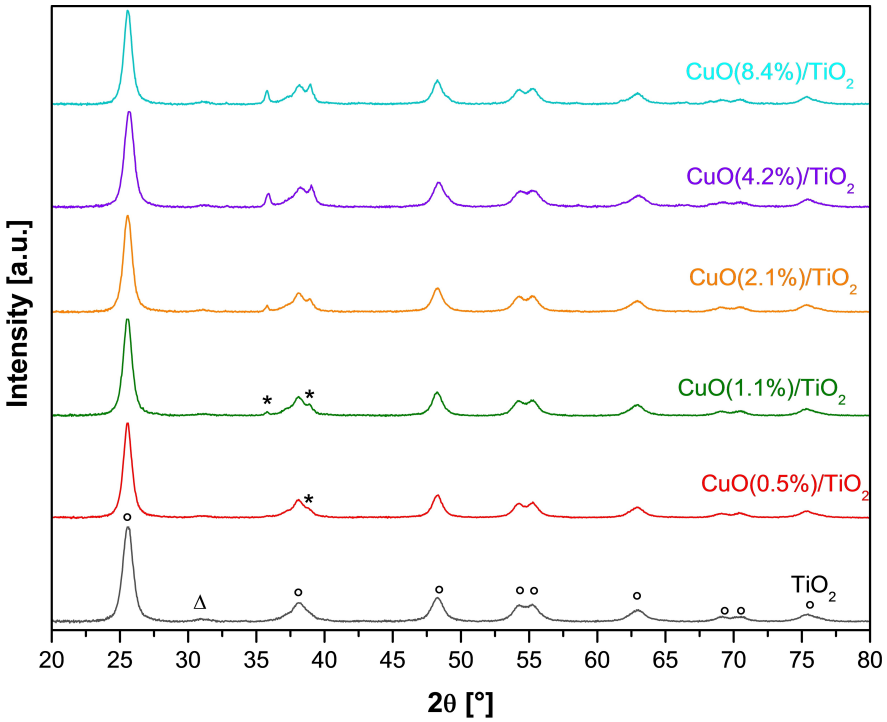

Figure 2. XRD patterns of the TiO_2 and Cu_xO/TiO_2 samples. The labels identify the main peaks of anatase (°), brookite (Δ) and CuO (*).

spectrum acquisition (not reported) we deduced the presence of C, O, Cu as expected from the composition of $Cu(CH_3COO)_2$). Going deeper into the chemical state of Cu, we acquired HR spectra in the region of the Cu2p doublet (see Figure 3). The shape and position of this 2p doublet are those known and reported in the literature[37] for the oxidation state of Cu(II), which is easily recognizable by the presence of the shake-up satellite between 940 and 950 eV, for the Cu2p3/2 component. We therefore have the confirmation that the Cu precursor is in the +2 oxidation state. Taking this as a reference, we moved on

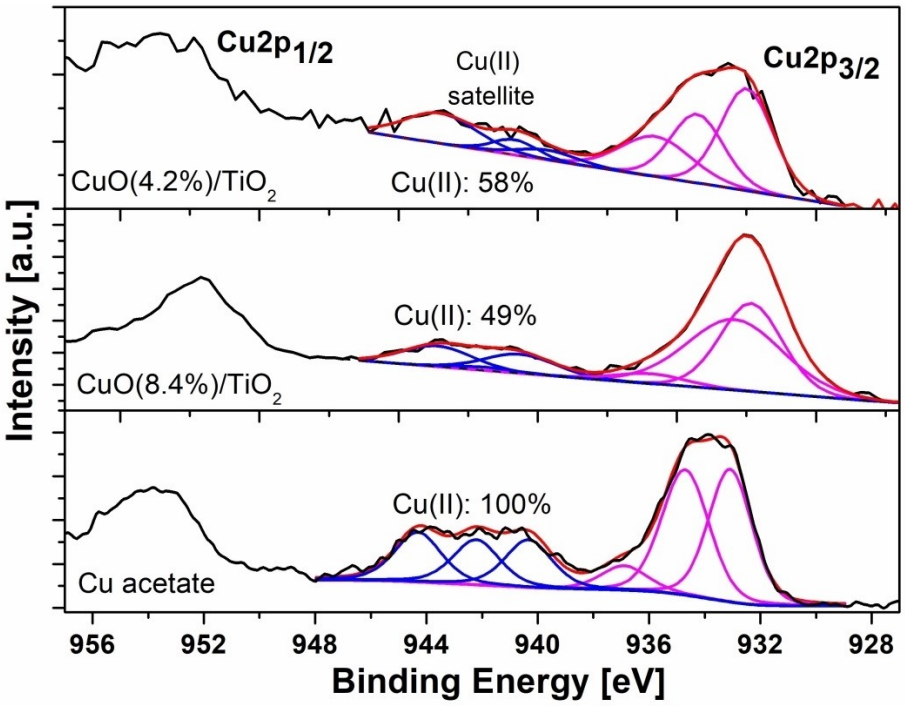

Figure 3. XPS Cu2p HR regions for samples (top) CuO(4.2%)/TiO_2, (middle) CuO(8.4%)/TiO_2 and (down) Cu acetate. A fitting procedure was applied to each $Cu2p_{3/2}$ peak and its satellite, to infer their area ratios, to be able to calculate the relative abundance of the Cu(II) oxidation state, according to [37].

to the Cu_xO-TiO_2 composite materials. We decided to check the CuO(4.2%)/TiO_2 and CuO(8.4)%/TiO_2 samples. The survey spectra (not shown) showed the presence of C, O, Cu and Ti, as expected. The HR regions of Cu2p (see Figure 3) show slightly different doublets, when compared to the previous one of Cu-acetate. The shake-up satellite is reduced in intensity for both samples, while the photoelectronic peaks show higher FWHM values, due to the presence of more than one oxidation state, since there is a shift towards lower binding energy for lower oxidation states: Cu(I) is predicted at 932.2 eV, while Cu(II) is usually found between 933.8–934.7 eV.[37]

To calculate the relative abundance of the Cu(II) component, for all three samples, we followed the method of M. C. Biesinger et al.,[37] which requires the evaluation of the $Cu2p_{3/2}$ peak area to be compared with the relative satellite area, by means of a fitting procedure, which has no chemical-physical meaning, since no component is attributed to each curve used to infer the peak total area. The procedure was applied to all spectra (as reported in Figure 3), and gave, as a result, for the Cu acetate sample an abundance of the Cu(II) oxidation state equal to 100%, while it gave 58% for CuO(4.2%)/TiO_2 and 49% for CuO(8.4%)/TiO_2. We then found, from XPS analysis, that the average oxidation state of Cu changes from sample to sample, with a total composition of 100% Cu(II) for the reference precursor Cu acetate.

Figure 4 depicts the Raman spectra evolution of all the analysed samples. Pure TiO_2 evidenced the Raman bands typical of TiO_2 in the anatase phase.[38] More in detail, the Raman bands at about 144 and 636 cm^{-1} are assigned to the symmetric stretching vibration of O–Ti–O,[36,39] while the signals at about 394 and 514 cm^{-1} are generated from the symmetric and anti-symmetric bending vibrations of O–Ti–O, respectively.[40] Pure CuO showed Raman bands at 291, 343, and 636 cm^{-1}, which well agree with the Raman analysis of CuO crystals reported in the literature.[41] The increase of CuO content in Cu_xO/TiO_2 photocatalysts resulted in a lower intensity of the TiO_2 Raman band at 144 cm^{-1} because of the dispersion of copper oxide nanoparticles on the TiO_2 surface, determining a sharing effect of the surface O entities[36,43] and indicating the possible formation of a heterojunction between TiO_2 and copper oxide. Furthermore, the presence of CuO on the TiO_2 surface was confirmed by the band formation at 291 cm^{-1}, which appeared

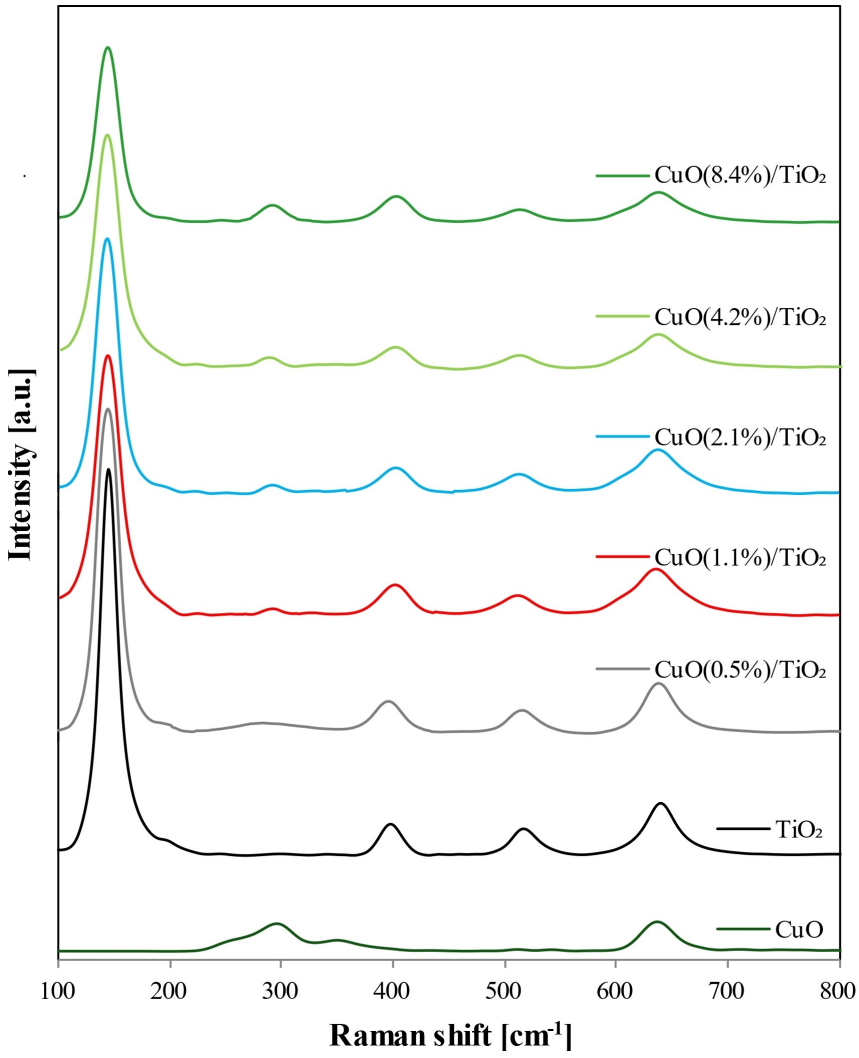

Figure 4. Raman spectra of Cu_xO/TiO_2 composites with respect to pure TiO_2 and CuO spectra.

more evident as the amount of CuO increased.[44] Therefore, the Raman spectroscopy results are fully consistent with the XRD analysis.

Table 1 shows the specific surface area (SSA) values of all the photocatalysts calculated through the BET method. The results highlighted that the highest SSA value is that of TiO_2 (79 $m^2 g^{-1}$), while bare CuO shows the lowest value (9 $m^2 g^{-1}$). Furthermore, the SSA value decreases with the increase of the CuO load within the Cu_xO/TiO_2 composites. This behaviour may be due to the deposition of progressively increasing amounts of copper oxide on the surface of TiO_2, as reported in the literature.[45]

The UV-Vis DRS spectra of the photocatalysts in terms of Kubelka-Munk function as a function of wavelength (in the range of 300–900 nm) are presented in Figure 5. As expected, bare TiO_2 exhibited a strong absorption feature below 400 nm, evidencing that this sample can absorb only in the UV-A region of the electromagnetic spectrum.[47] On the other hand, the presence of CuO in Cu_xO/TiO_2 composites induced a red shift of the absorption onset and the generation of additional absorption contributions in the range of 400–800 nm.[49] In detail, the absorption band extending from about 450 nm to about 550 nm is assigned to the electrons transfer from the valence band of TiO_2 to the conduction band of CuO.[36,50] Such optical absorption can be evidence for the generation of a heterojunction between CuO and TiO_2 in the Cu_xO/TiO_2 composites. Additonally, the broad band located in the range of 700–800 nm is associated with the d–d transition of Cu^{2+} of bulk copper oxide particles.[36,50–51]

Table 1. Specific surface area (*SSA*) and optical energy band gap (E_{bg}) values for the synthetized photocatalyst in comparison with bare CuO.

Sample	*SSA* [$m^2 g^{-1}$]	E_{bg} [eV]
TiO_2	79.0	3.20
CuO(0.5 %)/TiO_2	78.0	3.10
CuO(1.1 %)/TiO_2	76.0	3.05
CuO(2.1 %)/TiO_2	75.0	3.00
CuO(4.2 %)/TiO_2	74.0	2.87
CuO(8.4 %)/TiO_2	70.0	2.50
CuO	8.8	1.52

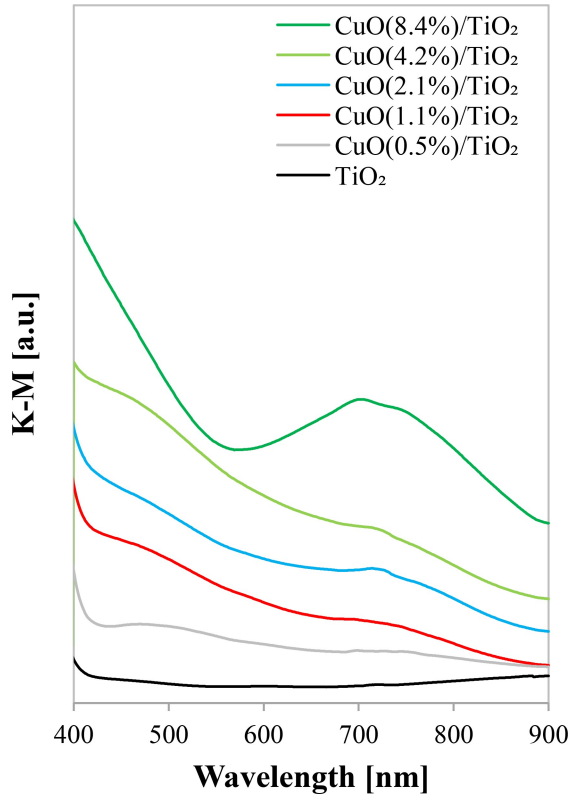

Figure 5. Kubelka-Munk function (K–M) values as a function of wavelength for TiO_2 and Cu_xO/TiO_2 composites.

The Tauc plot, which is used to determine the optical energy band gap (E_{bg}) of bare TiO_2, Cu_xO/TiO_2 composites and pure CuO, is depicted in Figure S5 (Supporting Information) while the obtained values of E_{bg} are reported in Table 1. The E_{bg} of pure TiO_2 and CuO was 3.20 and 1.52 eV, respectively. Compared to pure TiO_2, the E_{bg} of the Cu_xO/TiO_2 photocatalysts decreased with the increase of CuO content, in agreement with literature papers dealing with the formulation of copper oxide-based photocatalysts.[36,46,52] In particular, the E_{bg} of CuO(0.5 %)/TiO_2 was 3.1 eV and decreased up to 2.5 eV for the CuO(8.4 %)/TiO_2 sample (Table 1).

Photoluminescence spectra were acquired at an excitation length of 362 nm to follow the fate of the hole-electron pairs (Figure 6). The spectra show some characteristic titania peaks such as the one at 425 nm attributed to the radiative recombination of the self-trapped electrons (STE) and corresponding to the band gap of the titania anatase.[53] The extent of photogenerated electron trapping has a strong influence on the efficiency of photocatalytic systems and can cause a mismatch between the PL peak and the absorption edge (Stoke shift).[54] The mechanism of STE formation is complex and is attributed to the interaction between carriers and acoustic phonons.[56] However, Litke et al report that, in TiO_2, this

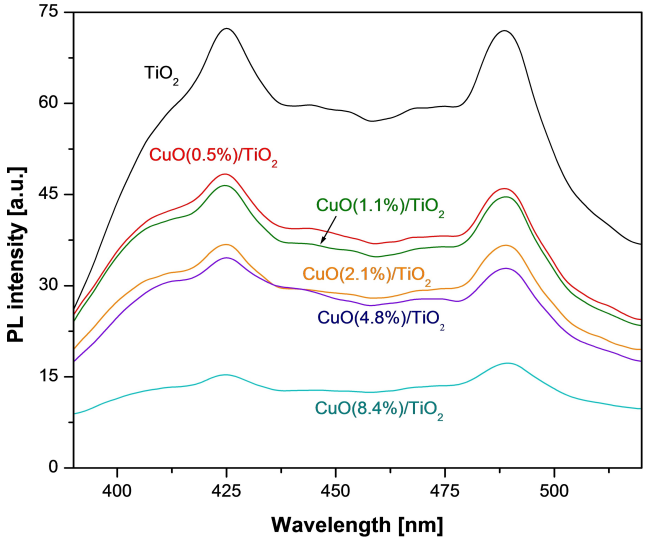

Figure 6. Photoluminescence spectra of bare TiO_2 and Cu_xO/TiO_2 samples.

mechanism has not been fully elucidated.[54] Another characteristic peak is the one at 490 nm, attributed to the oxygen vacancy with two trapped electrons, i.e. the F-center.[57] The gradual dropping of the PL intensity as the copper load increases is a sign of a more effective separation of electrons and photogenerated holes. This result can be explained by the transfer of electrons from TiO_2 to copper oxide nanoparticles at the interface,[36] in agreement with Raman and UV-Vis DRS results.

3.2. Photoepoxidation Activity Tests

3.2.1. Influence of Cu_xO Loading

To assess the influence of Cu_xO loading, the photoepoxidation activity tests of the prepared samples were performed by feeding 4000 ppm of C_3H_6 into the photoreactor (stoichiometric molar ratio, $F_R = c_{C3H6}^{IN}/c_{O2}^{IN} = 2$), irradiating the photocatalytic bed with a UV-A light intensity of 142 mW cm^{-2}, and using a mass of photocatalyst equal to 3.2 g.

Figure 7 shows the results of the photocatalytic epoxidation test on the CuO(1.1 %)/TiO_2 photocatalyst. After switching on the UV-A LEDs, a rapid increase in the conversion of propylene was observed due to the propylene partial desorption from the catalyst surface caused by the temperature increase from room temperature up to 40 °C. However, the propylene conversion became stable after 15 min of irradiation evidencing the reaching of the steady-state condition (Figure 7a). Simultaneously, the formation of PO was observed. After about 25 min of irradiation time, the PO concentration reached a steady state value. At this point, the LEDs were switched off and a decrease in propylene conversion and PO concentration was observed. During the irradiation period, CO_2 and CO were also detected (Figure 7b) and the steady state values were 710 and 15 ppm, respectively. No other products were detected during the overall irradiation time. The thermal effect on propylene conversion was assessed through a control test conducted at 40 °C without activating the light source, and the results confirmed that no propylene conversion occurred under these conditions.

The results of propylene photoepoxidation tests for all the tested photocatalysts are summarized in Table 2. Bare TiO_2 showed a propylene conversion of 14.8 % with a very low PO selectivity (lower than 3 %) and a very high selectivity to carbon oxides (higher than 97 %), underlining that in the absence of copper oxide, TiO_2 is not able to promote the selective formation of the epoxide. On the other hand, an increase in propylene conversion from 15.7–18.1 % was observed when the nominal CuO load in the composites increased from 0.5–1.1 wt % (i.e. for CuO(0.5 %)/TiO_2 and CuO(1.1 %)/TiO_2 photocatalysts, respectively). It is worthwhile noting that the PO selectivity and yield achieved with the CuO(1.1 %)/TiO_2 photocatalyst were 72 and 13 %, significantly higher than that observed for bare TiO_2. Since the amount of propylene adsorbed under dark conditions decreases with increasing CuO loading, the improved photoepoxidation performance can be solely ascribed to the role of Cu_xO, which, under irradiation, acts as an active phase that can promote the formation of hydrogen peroxide in situ from molecular O_2 (see the photogenerated charges transfer mechanism for the Cu_xO/TiO_2 composite reported below). Once generated, hydrogen peroxide is the main oxidant involved in the mechanism of the propylene epoxidation reaction, as widely reported in the literature.[58] On the other hand, an increase of CuO content from 1.1–8.4 wt % resulted in a decrease in propylene conversion from 18.1 %–5.9 %. This result can be explained by invoking a phenomenon also known as "shielding effect" and reported in several literature papers.[61] Probably, for CuO content higher than 1.1 wt %, the colored copper oxide may hinder the effective irradiation of the not-coverd TiO_2 surface (photon absorption competition).[64] It is also reported that CuO loadings higher than the optimal ones (i.e. able to induce the formation of an effective heterojunction interface) may generate potential recombination sites for the photogenerated charge carriers.[36,50,65] As a consequence, a worsening of the photocatalytic activity is obtained.

From the results of the tests, it emerged that the optimal sample was CuO(1.1 %)/TiO_2, since the highest PO yield value of 13 % was obtained for this photocatalyst without a dramatic change in PO selectivity (Figure 8). For this reason, the subsequent photoepoxidation activity tests were conducted using the CuO(1.1 %)/TiO_2 photocatalyst.

Table 2. Steady state values of propylene adsorption during dark phase, propylene conversion (X), selectivity (S) and yield (Y) to PO, and selectivity to CO + CO_2 (S_{CO+CO2}) for photoepoxidation tests under UV-A light by varying the CuO load in the photocatalysts.

Photocatalyst	CuO [wt %]	C_3H_6 Adsorbed [μmol g_{CAT}^{-1}]	*X* [%]	*S* [%]	*Y* [%]	S_{CO+CO2} [%]
TiO_2	0.0	5.5	14.8	2.7	0.4	97.3
CuO(0.5 %)/TiO_2	0.5	5.3	15.7	60.4	9.5	39.6
CuO(1.1 %)/TiO_2	1.1	5.0	18.1	72.0	13.0	28.0
CuO(2.1 %)/TiO_2	2.1	4.6	14.7	78.3	11.5	21.7
CuO(4.2 %)/TiO_2	4.2	4.4	8.5	76.1	6.5	23.9
CuO(8.4 %)/TiO_2	8.4	3.6	5.9	75.1	4.5	24.9

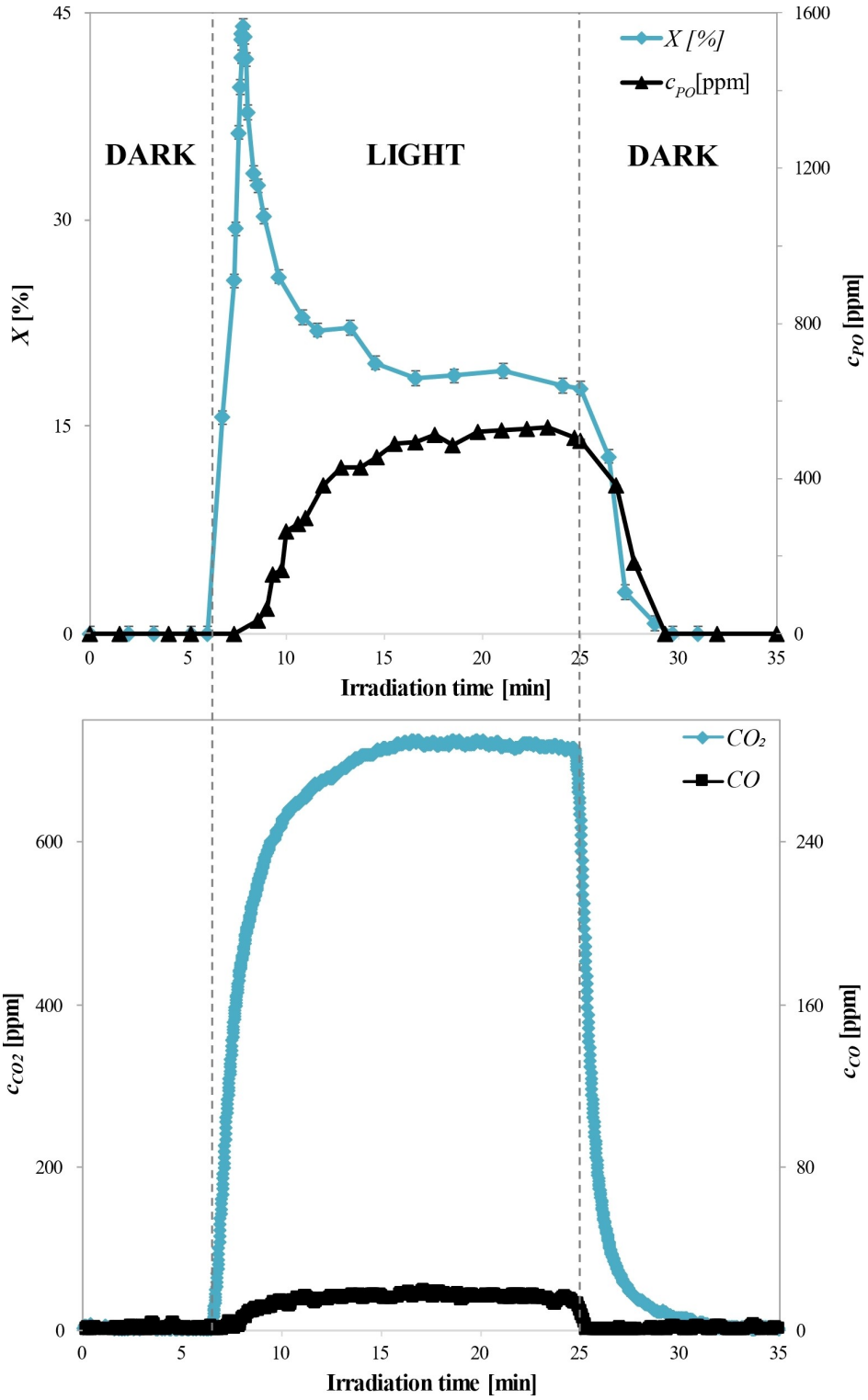

Figure 7. a) C_3H_6 conversion (X), C_3H_6O concentration, b) CO_2 and CO concentrations during the photoepoxidation test with CuO(1.1 %)/TiO_2 under UV-A light.

3.2.2. *Possible Reaction and Electron-Hole Transfer Mechanism at the Interface between CuO, Cu_2O and TiO_2*

The Mulliken relationship combined with the Nernst equation was applied to determine the edge positions of the valence band (E_{VB}) and conduction band (E_{CB}) at pH = 7 (vs NHE) for TiO_2 and CuO and Cu_2O[64,67]:

$$E_{VB} = X - E_c + \frac{1}{2} E_{bg} - 0.059^{*}7 \quad (5)$$

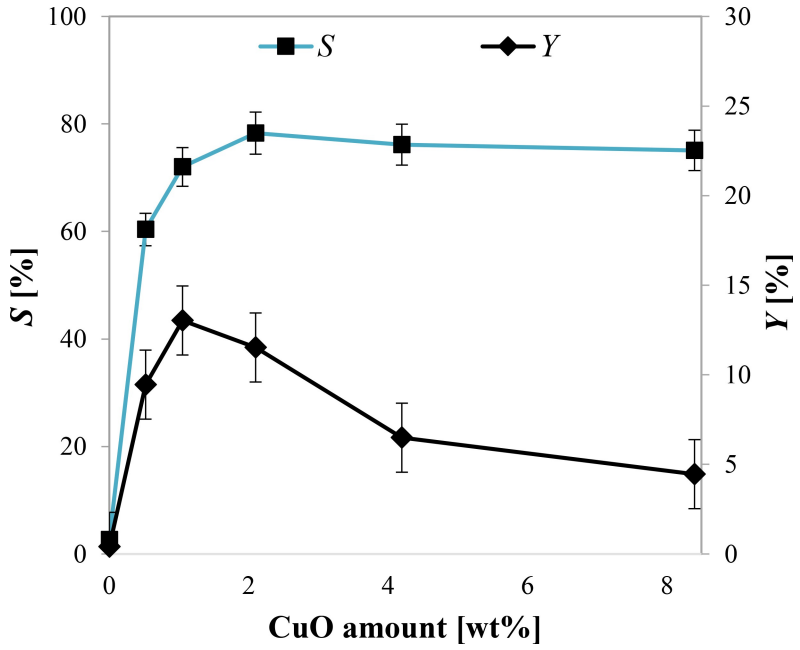

Figure 8. Steady state values of selectivity (S), and yield to PO (Y) for photoepoxidation tests under UV-A light by varying the CuO load in the Cu_xO/TiO_2 photocatalysts.

$$E_{CB} = E_{VB} - E_{bg} \quad (6)$$

where X is the absolute electronegativity of TiO_2 (5.81 eV), CuO (5.81 eV),[69] and Cu_2O (5.33 eV),[71] E_c is the energy of free electrons on the hydrogen scale (ca. 4.5 eV), and E_{bg} is the band gap energy of the TiO_2 (3.2 eV), CuO (1.52 eV) obtained from UV-Vis DRS analysis (Table 1), and Cu_2O (1.99 eV).[71] Taking into account the results and the works reported in the literature,[72] the charge transfer (electrons and holes) in Cu_xO/TiO_2 composite photocatalysts, considering the couple TiO_2-Cu_2O and TiO_2-CuO, could be classified as a straddling gap (type I).[75] Indeed, the E_{VB} and E_{CB} of TiO_2 are 2.5 V (vs NHE at pH = 7) and −0.7 V (vs NHE at pH = 7), the E_{VB} and E_{CB} of Cu_2O are 1.41 V (vs NHE at pH = 7) and −0.58 V (vs NHE at pH = 7), while the E_{VB} and E_{CB} of CuO are 1.66 V (vs NHE at pH = 7) and 0.14 V (vs NHE at pH = 7), respectively, achieving the band alignment reported in Figure 9.

As shown from UV-Vis DRS spectra, Cu_xO/TiO_2 composite is able to absorb UV-A light (Equation (7)). At the CuO/TiO_2 interface, the photogenerated holes transfer from the TiO_2 valence band (VB) to the CuO VB and subsequently to the Cu_2O VB. Simultaneously, the electrons that are promoted in the TiO_2 conduction band (CB) moved into the Cu_2O CB, and finally to CuO CB. Since the $O_2/O_2^{-}\cdot$ redox potential (−0.35 V vs NHE at pH = 7[76]) is more negative than the E_{CB} of CuO, the electrons in the CuO CB cannot reduce molecular oxygen to superoxide. On the other hand, since the CuO E_{CB} (+0.14 V vs NHE at pH = 7) is less positive than the redox potential of O_2/H_2O_2 (+0.28 V vs NHE at pH = 7), the electrons in the CuO CB are able to reduce O_2 to H_2O_2 involving H^+ (Equation (9)[76]) that transfers from the hole site to the electron site thanks to proton hopping and/or proton diffusion events.[79]

However, the holes in the TiO_2 VB can oxidize the adsorbed H_2O to generate hydroxyl radicals (Equation (8)) because the redox potential of the OH·/H_2O pair (+2.31 V vs NHE at pH = 7[76]) is less positive than the E_{VB} of TiO_2 (+2.5 V vs NHE at pH = 7) whereas the holes in the Cu_2O VB cannot generate hydroxyl radicals from water since the E_{VB} of Cu_2O (+1.41 V vs NHE at pH = 7) is less positive than of OH·/H_2O pair. Therefore, the generated hydrogen peroxide (Equation (9)) allows the epoxidation of adsorbed propylene (Equation (10)).[2,58] Simultaneously, the oxidation of propylene to CO_2 can occur via positive holes and hydroxyl radicals (Equation 11).[81]

$$Cu_xO/TiO_2 + h\nu \rightarrow h^+ + e^- \quad (7)$$

$$h^+ + H_2O_{(ads)} \rightarrow OH^\bullet + H^+ \quad (8)$$

$$2e^- + O_2 + 2H^+ \rightarrow H_2O_2 \quad (9)$$

$$C_3H_{6(ads)} + H_2O_2 \rightarrow C_3H_6O + H_2O \quad (10)$$

$$C_3H_{6(ads)} + OH^\bullet/h^+ \rightarrow intermediates \rightarrow CO_2 + H_2O \quad (11)$$

An additional photoepoxidation test was performed with the CuO(1.1%)/TiO_2 photocatalyst under the same operating conditions but in the absence of water to confirm the key role of hydrogen peroxide in the generation of PO. The results obtained from this test are shown in Figure 10. When the UV-A LEDs were turned on, the steady-state propylene conversion was about 6% and only carbon oxides were detected with a selectivity higher than 99%. Such a result is a clear indication that the positive holes are also involved in the mechanism that leads to the mineralization of propylene since the formation of

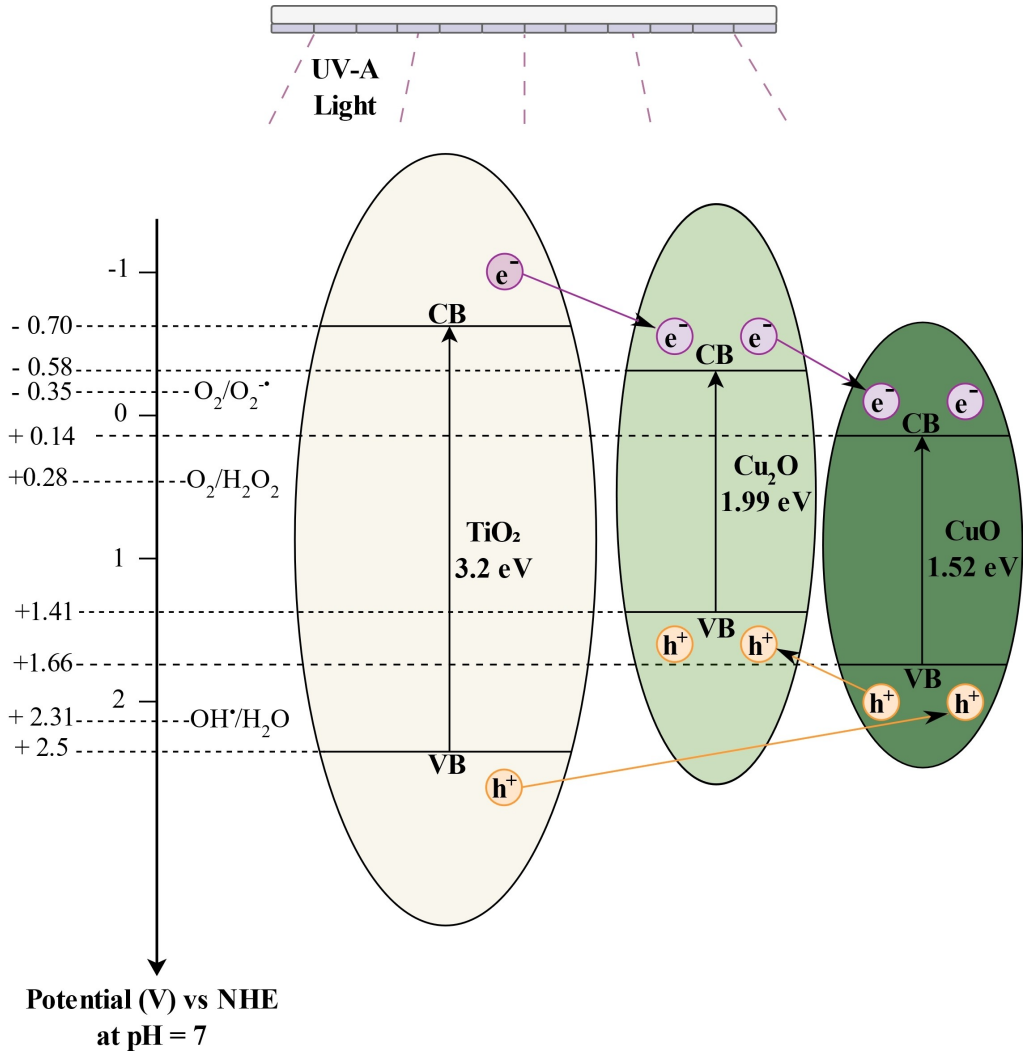

Figure 9. Proposed mechanism for electron and hole transfer in propylene photoepoxidation under UV-A light irradiation.

hydroxyl radicals (Equation (8)) does not occur when water is not continuously present in the reaction medium. Furthermore, the epoxide selectivity recorded in the overall irradiation time was negligible. Based on the latter result, it is possible to argue that the propylene epoxidation reaction can selectively occur only when hydrogen peroxide is in situ produced under irradiation. Indeed, in the absence of water in the gaseous stream, the hydroxyl radical formation cannot be generated and therefore H^+ is not formed (Equation (8)). As a consequence, hydrogen peroxide generation cannot occur through the reaction involving molecular O_2 and H^+ (Equation (9)).

Other tests were carried out to evaluate the activation of the CuO(1.1%)/TiO_2 photocatalyst with visible light and to analyze the generation of hydrogen peroxide by the photocatalyst. The results of the epoxidation tests in the presence of visible light showed that the CuO(1.1%)/TiO_2 photocatalyst cannot be efficiently excited for the generation of H_2O_2 (Figure S6 of Supporting Information). Indeed, in this case, PO was not detected, while the obtained propylene conversion was approximately 5% with the formation of only CO and CO_2. Possibly, propylene was oxidized to CO and CO_2 (Equation (12)) by the positive holes generated in the VB of Cu_2O. On the other hand, the non-formation of PO can be explained considering that only CuO and Cu_2O in CuO(1.1%)/TiO_2 can be excited by visible light (CuO E_{bg} = 1.52 eV; Cu_2O E_{bg} = 1.99 eV), and this does not allow the formation of H_2O_2 because the E_{VB} of Cu_2O (+1.41 V vs NHE at pH = 7) is less positive than of $OH^{\bullet}/H_2O$ pair. Consequently, under visible light, the H^+ necessary for the formation of H_2O_2 from O_2 cannot be generated (Equation (9)).

On the other hand, the tests for the evaluation of the generation of hydrogen peroxide demonstrated the formation of this oxidizing agent by CuO(1.1%)/TiO_2 photocatalyst under UV-A light. Indeed, from the spectrophotometric analysis, a continuous increase of the hydrogen peroxide absorbance signal during the irradiation time was observed (Figure S7 of Supporting Information). It is worthwhile to note that in the case of pure TiO_2, the generated H_2O_2 was significantly lower, in agreement with the literature.[83] This last result may explain the very low PO selectivity (lower than 3%) observed during the

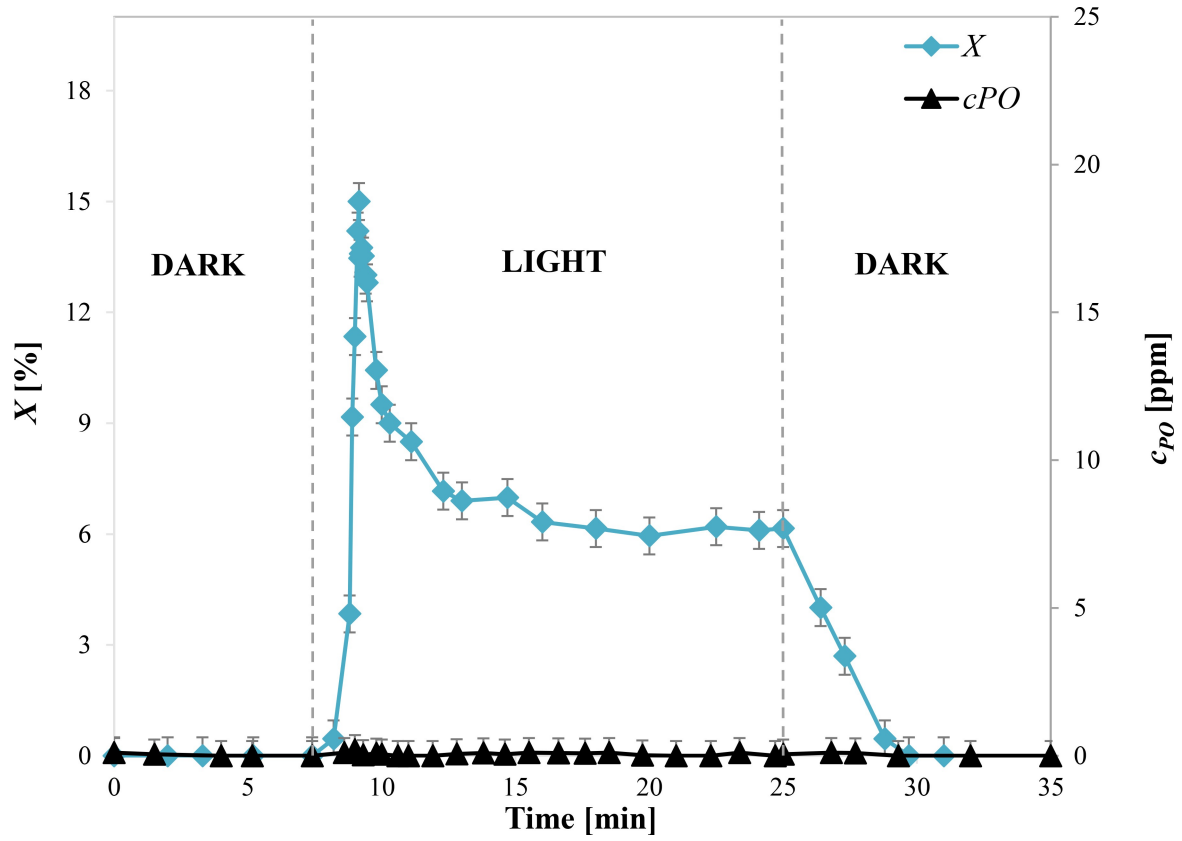

Figure 10. C_3H_6 conversion (X) and PO concentration (c_{PO}) in the photocatalytic test with CuO(1.1 %)/TiO_2 under UV-A light in the absence of H_2O.

photoepoxidation test with TiO_2 alone under UV-A light (Table 2).

3.2.3. *Influence of the Incident UV-A Light Intensity*

Additional propylene photoepoxidation tests were carried out to evaluate the influence of the intensity of the UV-A light incident on the surface of the photocatalyst. The light intensity (Φ) was varied in the range of 72–320 mW cm^{-2}. The results are shown in Table 3 and Figure 10.

The experimental results evidenced that with the increase of Φ up to 297.2 mW cm^{-2}, the conversion of propylene increased linearly up to the value of 31.5 % (Figure 11a), while the further increase of the Φ did not favour the kinetics, since at higher photon flux values, the recombination reaction of the photoexcited pairs is favoured, worsening the photocatalytic activity.[85] On the other hand, the PO selectivity did not change significantly with the increase in incident light intensity (Figure 11b). Consequently, since the propylene conversion increased, the PO yield was enhanced up to achieve a value equal to 22.7 %.

Table 3. Steady-state values of propylene conversion, selectivity and yield to propylene oxide, and selectivity to CO and CO_2 for photoepoxidation tests by varying the incident UV-A light intensity.

Φ [mW cm^{-2}]	X [%]	S [%]	Y [%]	S_{CO+CO2} [%]
0	0.0	0.0	0.0	0.0
72	8.6	75.4	6.5	24.6
142	18.1	72.0	13.0	28.0
297.2	31.5	70.4	22.2	29.6
311.4	32.2	70.6	22.7	29.4
320	31.9	70.8	22.6	29.2

3.2.4. *Stability Test of the CuO(1.1 %)/TiO_2 Photocatalyst*

To evaluate the stability of the CuO(1.1 %)/TiO_2 photocatalyst, an irradiation test of 24 h was carried out under an incident UV-A light intensity of 297.2 mW cm^{-2}. The obtained results are shown in Figure 12.

It is possible to observe that the conversion of propylene and the PO yield increased in about 15 min to a steady state value and remained constant during all the photocatalytic tests showing the absence of any deactivation phenomena.

3.2.5. *Electric Energy Consumption and Comparison With the Literature*

Using the data collected from the photocatalytic tests, it was possible to calculate the electric energy consumption (E_M),

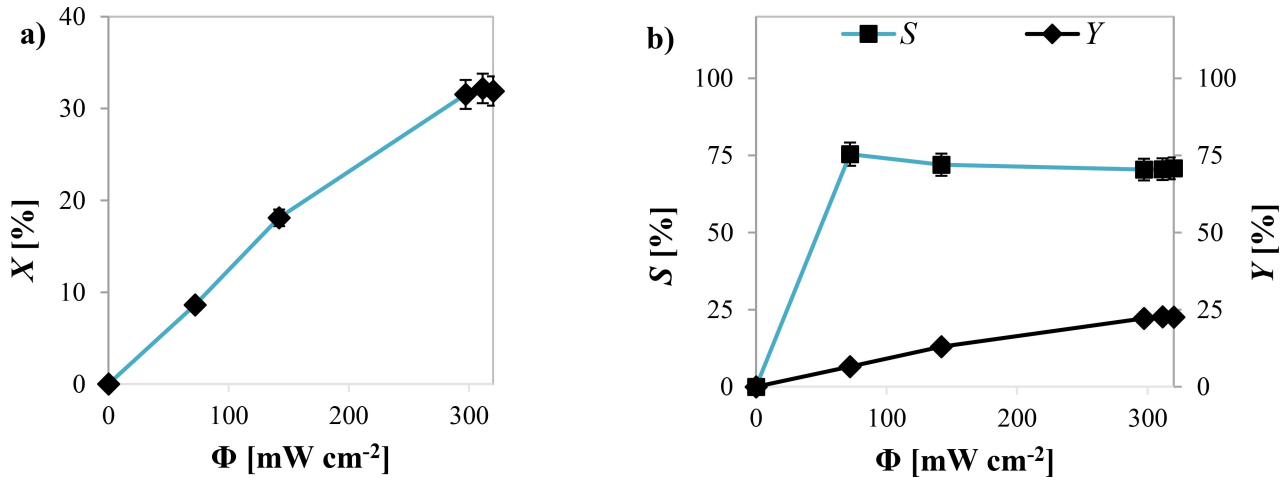

Figure 11. a) Steady-state values of propylene conversion (*X*) for photoepoxidation tests by varying the incident UV-A light intensity on CuO(1.1 %)/TiO_2; b) steady-state values of selectivity (*S*), and yield to propylene oxide (*Y*) for photoepoxidation tests by varying the incident light intensity on CuO(1.1 %)/TiO_2).

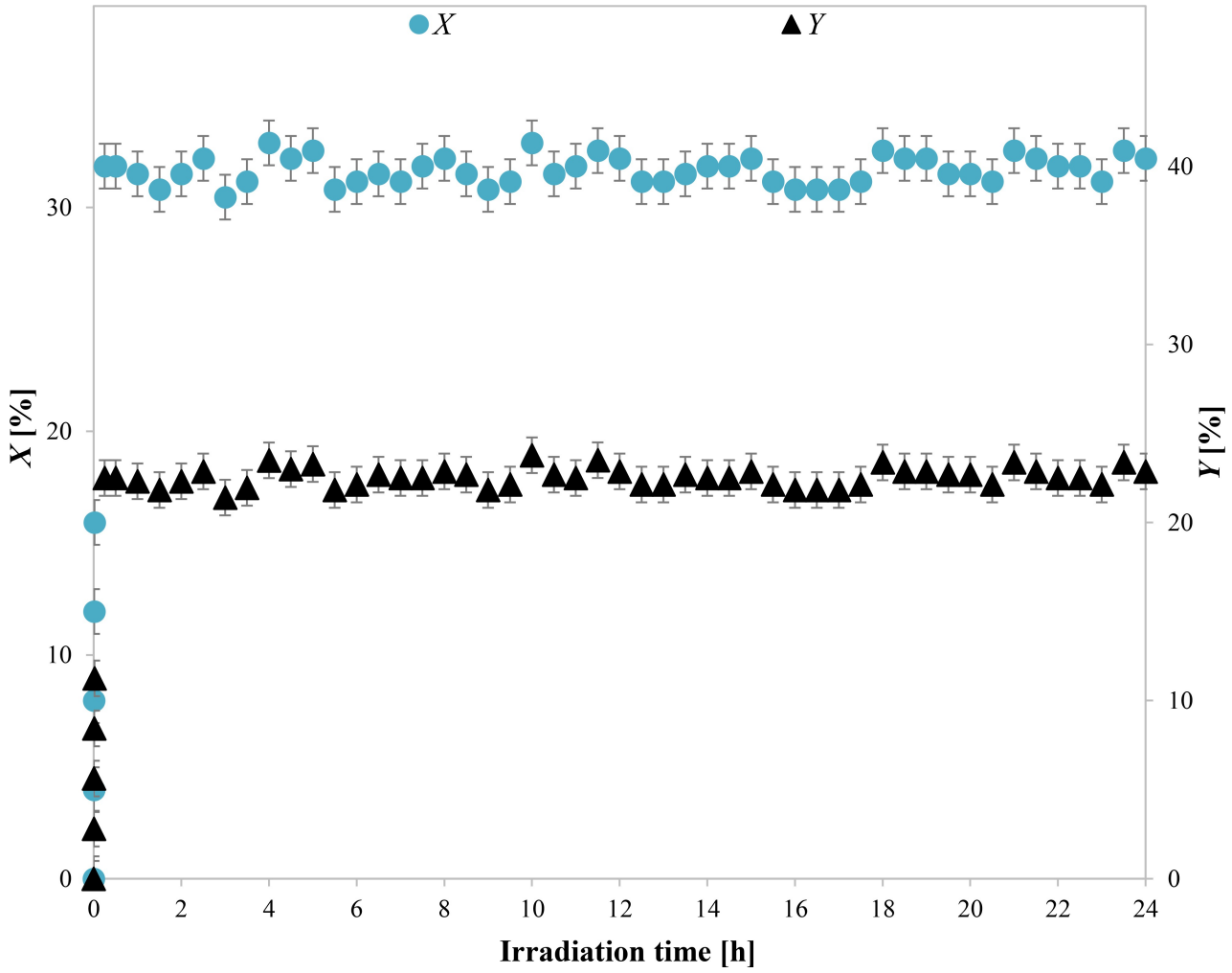

Figure 12. Propylene conversion and PO yield as a function of irradiation time. Photocatalyst weight: 3.2 g; gas flow rate: 30 L h^{-1} (STP); propylene inlet concentration: 4000 ppm; oxygen inlet concentration: 2000 ppm; water inlet concentration: 1000 ppm; incident UV-A light intensity: 297.2 mW cm^{-2}.

using the empirical equation proposed by Bolton et al.,[86] as reported below:

Table 4. Comparison with literature papers dealing with different photocatalysts for propylene epoxidation. PBPR = fixed bed photocatalytic reactor; FBPR = fluidized bed photocatalytic reactor.

Photocatalyst	Type of Reactor	UV-A Light	F_{C3H6}^{IN} [mol h^{-1}]	X [%]	Y [%]	P [kW]	E_{sp} [kW h mol_{C3H6}^{-1}]	Ref.
V0.2/MCM-41	PBPR	0.3 mW cm^{-2} (200 W Xe lamp)	2.65	0.07	0.016	0.2	107.82	[15]
V0.2Ti0.3/MCM-41	PBPR	0.3 mW cm^{-2} (200 W Xe lamp)	2.65	0.16	0.077	0.2	47.17	[15]
Ti0.3/MCM-41	PBPR	0.3 mW cm^{-2} (200 W Xe lamp)	2.65	0.01	0.007	0.2	754.72	[15]
Rb ion-modified 1.5% (wt) V_2O_5/SiO_2	PBPR	1.6 mW cm^{-2} (300 W Xe lamp)	0.011	1.56	0.438	0.3	1748.25	[87]
TiO_2	PBPR	(Philips SP 500-W Hg Lamp)	0.01	5.5	0.578	4.3	7818.18	[88]
ZrO_2	PBPR	(Philips SP 500-W Hg Lamp)	0.01	5	0.25	6.3	12600.00	[88]
BiWO–Ti50i/Glass Spheres	FBPR	90 mW cm^{-2} (40 UV-A LEDs, 100 W)	5.4	10	5.2	0.1	0.19	[23]
CuO(1.1%)/TiO_2	FBPR	297.2 mW cm^{-2} (240 LEDs, 100 W)	5.4	31.5	22.2	0.057	0.034	This work

$$E_M = \frac{P}{F^{IN}_{C_3H_6} * X} \quad (12)$$

Where P is the electric power of the light source (kW), $F^{IN}_{C_3H_6}$ is the molar flow rate of propylene in the inlet stream (mol_{C3H6} h^{-1}), and X is the propylene conversion at state steady condition.

Several papers have been identified in the literature on the synthesis of PO through a photocatalytic process based on the use of photocatalytic reactors operating in continuous mode. Their operating parameters and energy consumption are shown in Table 4 and compared with the results obtained in our work. It is possible to observe that the use of the CuO(1.1%)/TiO_2 in a photocatalytic fluidized bed reactor is the most advantageous in terms of energy saving since the lowest E_M is achieved. Furthermore, in all cases, the propylene conversion and PO yield were in the range of 0.01–10% and 0.007–5.2%, respectively, significantly lower than that of CuO(1.1%)/TiO_2 photocatalyst (propylene conversion: 31.5%; PO yield: 22.2%).

4. Conclusions

Propylene epoxidation with molecular oxygen has been carried out with Cu_xO/TiO_2 composites in a fluidized-bed reactor under UV-A irradiation. The Cu_xO/TiO_2 composites at different CuO nominal loads (in the range 0.5–8.4 wt%) were simply prepared through thermal annealing of physical mixtures between copper acetate and sol-gel derived TiO_2. Physical-chemical characterization results confirmed the presence of Cu_xO in the composites and the possible formation of a heterojunction between TiO_2 and copper oxide.

Photoepoxidation tests showed that the addition of Cu_xO on the TiO_2 surface led to an increase in propylene conversion and selectivity to propylene oxide. In particular, the best performances (propylene conversion: 18.1%; propylene epoxide selectivity: 72%) were obtained when the CuO nominal load was 1.1%. It was argued that CuO in the Cu_xO/TiO_2 composite promotes the transformation of molecular O_2 into hydrogen peroxide that, in turn, is able to directly oxidize propylene to propylene oxide. Moreover, the use of an incident UV-A light intensity of 297.2 mW cm^{-2} allowed to reach a propylene conversion and epoxide yield of 31.5 and 22.2%, respectively, significantly higher than that reported in the literature dealing with the propylene epoxidation in photocatalytic reactors operating in continuous mode. In addition, the stability of the optimal photocatalyst was evaluated by a 24 h photocatalytic activity test, showing the absence of deactivation phenomena and underlining that the Cu_xO/TiO_2 composite with a nominal CuO content of 1.1 wt% can be considered an effective and selective photocatalyst for the direct photocatalytic epoxidation of propylene with molecular oxygen, allowing also a significant energy saving.

Conflict of Interests

The authors declare no conflict of interest.

Data Availability Statement

The data that support the findings of this study are available from the corresponding author upon reasonable request.

Keywords: Propylene · Photoepoxidation · Propylene oxide · Fluidized bed photoreactor · Cu_xO/TiO_2

[1] H. Baer, M. Bergamo, A. Forlin, L. H. Pottenger, J. Lindner, Propylene Oxide, in *Ullmann's Encyclopedia of Industrial Chemistry* **2000**, https://doi.org/10.1002/14356007.a22_239.pub3.
[2] X. Wang, P. Zhou, Q. Zhou, Q. Zhang, H. Ning, M. Wu, W. Wu, *Chem. Eng. J.* **2023**, *476*, 146488.
[3] Z. Song, X. Feng, N. Sheng, D. Lin, Y. Li, Y. Liu, X. Chen, D. Chen, X. Zhou, C. Yang, *Chem. Eng. J.* **2019**, *377*, 119927.
[4] L. Wang, J. Dai, Y. Xu, Y. Hong, J. Huang, D. Sun, Q. Li, *J. Mater. Chem. A* **2020**, *8*, 4428–4436.
[5] W. Xiong, X.-K. Gu, Z. Zhang, P. Chai, Y. Zang, Z. Yu, D. Li, H. Zhang, Z. Liu, W. Huang, *Nat. Commun.* **2021**, *12*, 5921.
[6] D. Kahlich, U. Wiechern, J. Lindner, Wiley-VCH, Weinheim, Cambridge, **2003**, Propylene Oxide, in *Ullmann's Encyclopedia of Industrial Chemistry*, Vol. 30.
[7] J. Tsuji, J. Yamamoto, M. Ishino, N. Oku, *Sumitomo Kagaku* **2006**, *1*, 4–10.
[8] J. Yamamoto, C. Works, H. Koike, S. Yoshida, *Sumitomo Kagaku Rep.* **2019**, 2019, 1–9.
[9] M. Signorile, V. Crocellà, A. Damin, B. Rossi, C. Lamberti, F. Bonino, S. Bordiga, *J. Phys. Chem. C* **2018**, *122*, 9021–9034.
[10] S. J. Khatib, S. Oyama, *Catal. Rev.* **2015**, *57*, 306–344.
[11] M. Lin, C. Xia, B. Zhu, H. Li, X. Shu, *Chem. Eng. J.* **2016**, *295*, 370–375.
[12] V.-H. Nguyen, B.-S. Nguyen, H.-T. Vo, C. C. Nguyen, S.-R. Bae, S. Y. Kim, Q. V. Le, *Catalysts* **2020**, *10*, 87.
[13] J. Rouchaud, M. De Pauw, *J. Catal.* **1969**, *14*, 114–117.
[14] Y. Liu, K. Murata, M. Inaba, N. Mimura, *Appl. Catal., B* **2005**, *58*, 51–59.
[15] V.-H. Nguyen, S. D. Lin, J. C.-S. Wu, *J. Catal.* **2015**, *331*, 217–227.
[16] P. Khemthong, P. Photai, N. Grisdanurak, *Int. J. Hydrog. Energy* **2013**, *38*, 15992–16001.
[17] J. Yu, Y. Hai, M. Jaroniec, *J. Colloid Interface Sci.* **2011**, *357*, 223–228.
[18] P. Ciambelli, D. Sannino, V. Palma, V. Vaiano, R. S. Mazzei, *Int. J. Photoenergy* **2009**, *2009*, 709365-709371.
[19] D. Sannino, V. Vaiano, P. Ciambelli, P. Eloy, E. M. Gaigneaux, *Appl. Catal., A* **2011**, *394*, 71–78.
[20] V. Palma, D. Sannino, V. Vaiano, P. Ciambelli, *Ind. Eng. Chem. Res.* **2010**, *49*, 10279–10286.
[21] D. Sannino, V. Vaiano, P. Ciambelli, *Catal. Today* **2013**, *205*, 159–167.
[22] D. Sannino, V. Vaiano, P. Ciambelli, J. Murcia, M. Hidalgo, J. A. Navío, *J. Adv. Oxid. Technol.* **2013**, *16*, 71–82.
[23] S. Murcia-López, V. Vaiano, D. Sannino, M. Hidalgo, J. Navío, *Res. Chem. Intermed.* **2015**, *41*, 4199–4212.
[24] G. Bagnasco, C. Cammarano, M. Turco, S. Esposito, A. Aronne, P. Pernice, *Thermochim. Acta* **2008**, *471*, 51–54.
[25] S. Esposito, in *Sol-Gel Synthesis Strategies for Tailored Catalytic Materials*, Springer Nature Switzerland AG, **2023**, pp. 13–20.
[26] D. Manoj, S. Rajendran, M. Naushad, M. Santhamoorthy, F. Gracia, M. S. Moscoso, M. Gracia-Pinilla, *Environ. Res.* **2023**, *216*, 114428.
[27] P. Ciambelli, D. Sannino, V. Palma, V. Vaiano, *Int. J. Photoenergy* **2008**, *2008*, https://doi.org/10.1155/2008/258631.
[28] D. Sannino, V. Vaiano, P. Ciambelli, G. Carotenuto, M. Di Serio, E. Santacesaria, *Catal. Today* **2013**, *209*, 159–163.
[29] G. Eisenberg, *Ind. Eng. Chem. Anal. Ed.* **1943**, *15*, 327–328.
[30] R. M. Sellers, *Analyst* **1980**, *105*, 950–954.
[31] A. Mancuso, N. Blangetti, O. Sacco, F. S. Freyria, B. Bonelli, S. Esposito, D. Sannino, V. Vaiano, *Nanomaterials* **2023**, *13*, 270.
[32] L. Andronic, D. Andrasi, A. Enesca, M. Visa, A. Duta, *J. Sol-Gel Sci. Technol.* **2011**, *58*, 201–208.
[33] B. Bonelli, O. Tammaro, F. Martinovic, R. Nasi, G. Dell'Agli, P. Rivolo, F. Giorgis, N. Ditaranto, F. A. Deorsola, S. Esposito, *ACS Omega* **2021**, *6*, 24562–24574.
[34] J. Huang, S. Wang, Y. Zhao, X. Wang, S. Wang, S. Wu, S. Zhang, W. Huang, *Catal. Commun.* **2006**, *7*, 1029–1034.
[35] G. V. Sagar, P. V. R. Rao, C. S. Srikanth, K. V. Chary, *J. Phys. Chem. B* **2006**, *110*, 13881–13888.
[36] Q. Shi, G. Ping, X. Wang, H. Xu, J. Li, J. Cui, H. Abroshan, H. Ding, G. Li, *J. Mater. Chem. A* **2019**, *7*, 2253–2260.
[37] M. C. Biesinger, B. R. Hart, R. Polack, B. A. Kobe, R. S. C. Smart, *Miner. Eng.* **2007**, *20*, 152–162.
[38] J. Liu, C. Han, X. Yang, G. Gao, Q. Shi, M. Tong, X. Liang, C. Li, *J. Catal.* **2016**, *333*, 162–170.
[39] P. Yang, M. Douthwaite, J. Pan, L. Zheng, S. Hong, D. J. Morgan, M. Gao, D. Li, J. Feng, G. J. Hutchings, *Catal. Sci. Technol.* **2021**, *11*, 4898–4910.
[40] Q. Shi, Y. Li, Y. Zhou, S. Miao, N. Ta, E. Zhan, J. J. Liu, W. Shen, *J. Mater. Chem. A* **2015**, *3*, 14409–14415.
[41] T. H. Nguyen, T. L. Nguyen, T. D. T. Ung, Q. L. Nguyen, *Adv. Nat. Sci.: Nanosci. Nanotechnol.* **2013**, *4*, 025002.
[42] P. S. Murthy, V. Venugopalan, D. D. Arunya, S. Dhara, R. Pandiyan, A. Tyagi, in *International Conference on Nanoscience, Engineering and Technology (ICONSET 2011)*, IEEE, **2011**, pp. 580–583, doi: 10.1109/ICONSET.2011.6168037.
[43] M. Golestanbagh, M. Parvini, A. Pendashteh, *Catal. Lett.* **2018**, *148*, 2162–2178.
[44] M. Chen, Y. Liu, W. Zhou, P. Wu, *Ceram. Int.* **2023**, *49*, 7676–7682.
[45] H. Nishikiori, N. Harata, S. Yamaguchi, T. Ishikawa, H. Kondo, A. Kikuchi, T. Yamakami, K. Teshima, *Catalysts* **2019**, *9*, 383.
[46] F. Yang, M. Liu, X. Chen, Z. Xu, H. Zhao, *Sol. RRL* **2018**, *2*, 1800215.
[47] A. Mancuso, N. Morante, M. De Carluccio, O. Sacco, L. Rizzo, M. Fontana, S. Esposito, V. Vaiano, D. Sannino, *Chem. Eng. J.* **2022**, *450*, 138107.
[48] A. Mancuso, O. Sacco, D. Sannino, S. Pragliola, V. Vaiano, *Arabian J. Chem.* **2020**, *13*, 8347–8360.
[49] M. Wang, S. Fan, X. Li, J. Shi, Y. Mao, Y. Yang, G. Li, *ACS Appl. Mater. Interfaces* **2024**, *16*, 5735–5744.
[50] L. Li, X. Chen, X. Quan, F. Qiu, X. Zhang, *ACS Omega* **2023**, *8*, 2723–2732.
[51] Y. Zeng, T. Wang, S. Zhang, Y. Wang, Q. Zhong, *Appl. Surf. Sci.* **2017**, *411*, 227–234.
[52] D. A. Giannakoudakis, A. Qayyum, V. Nair, A. Khan, S. R. Pradhan, J. Prekodravac, K. Rekos, A. P. LaGrow, O. Bondarchuk, D. Łomot, *Mol. Catal.* **2021**, *514*, 111664.
[53] S. Abdullah, M. Sahdan, N. Nafarizal, H. Saim, A. Bakri, C. Cik Rohaida, F. Adriyanto, Y. Sari, *J. Phys.: Conf. Ser.* **2018**, *995*, 012067.
[54] A. Litke, E. J. Hensen, J. P. Hofmann, *J. Phys. Chem. C* **2017**, *121*, 10153–10162.
[55] N. Ali, X. Wang, H. Wu, in *Modeling, Characterization, and Production of Nanomaterials*, Elsevier, **2023**, pp. 437–466, https://doi.org/10.1016/B978-0-12-819905-3.00016-6.
[56] S. R. Rondiya, R. A. Jagt, J. L. MacManus-Driscoll, A. Walsh, R. L. Hoye, *Appl. Phys. Lett.* **2021**, *119*, https://doi.org/10.1063/5.0071763.
[57] N. Morante, O. Tammaro, L. Albarano, L. De Guglielmo, N. Oliva, O. Sacco, A. Mancuso, M. Castellino, D. Sannino, N. Femia, *Chem. Eng. J.* **2024**, *482*, 149175.
[58] M. Ko, Y. Kim, J. Woo, B. Lee, R. Mehrotra, P. Sharma, J. Kim, S. W. Hwang, H. Y. Jeong, H. Lim, *Nat. Catal.* **2022**, *5*, 37–44.
[59] F. Amano, T. Tanaka, *Chem. Lett.* **2006**, *35*, 468–473.
[60] R. Xu, H. Huang, W. Wang, L. Ding, Q. Lin, J. Li, Y. Zhang, Y. Han, J. Wang, X. Lu, *Chem. Eng. J.* **2023**, *461*, 141748.
[61] H. W. Nasution, E. Purnama, S. Kosela, J. Gunlazuardi, *Catal. Commun.* **2005**, *6*, 313–319.
[62] E. Kowalska, S. Rau, B. Ohtani, *J. Nanotechnol.* **2012**, *2012*, https://doi.org/10.1155/2012/361853.
[63] K. Wang, Z. Wei, B. Ohtani, E. Kowalska, *Catal. Today* **2018**, *303*, 327–333.
[64] M. Janczarek, E. Kowalska, *Catalysts* **2017**, *7*, 317.
[65] F. Niu, D. Chen, L. Qin, N. Zhang, J. Wang, Z. Chen, Y. Huang, *ChemCatChem* **2015**, *7*, 3279–3289.
[66] Y. Li, W.-N. Wang, Z. Zhan, M.-H. Woo, C.-Y. Wu, P. Biswas, *Appl. Catal., B* **2010**, *100*, 386–392.
[67] A. Walsh, K. T. Butler, *Acc. Chem. Res.* **2014**, *47*, 364–372.
[68] R. S. Mulliken, *J. Chem. Phys.* **1934**, *2*, 782–793.
[69] M.-P. Mazhari, H. Khojasteh, N. Sharifi, P. Aspoukeh, S. M. Mousavi, *J. Sol-Gel Sci. Technol.* **2024**, 110(1), 1–13.
[70] S. A. Behera, A. Subhadarshini, S. S. Bhuyan, B. Nanda, P. G. R. Achary, *Inorg. Chem. Commun.* **2024**, *160*, 111995.
[71] T. Gao, T.-T. Li, X. Liao, J.-H. Lin, B.-C. Shiu, C.-W. Lou, *J. Mater. Res. Technol.* **2022**, *21*, 798–809.
[72] L. Dai, F. Sun, P. Fu, H. Li, *RSC Adv.* **2022**, *12*, 13381–13392.
[73] Y. Zhao, J. Chen, W. Cai, Y. Bu, Q. Huang, T. Tao, J. Lu, *Chem. Phys. Lett.* **2019**, *725*, 66–74.
[74] Y. Zhao, X. Linghu, Y. Shu, J. Zhang, Z. Chen, Y. Wu, D. Shan, B. Wang, *J. Environ. Chem. Eng.* **2022**, *10*, 108077.
[75] W. Hu, J. Yang, *J. Mater. Chem. C* **2017**, *5*, 12289–12297.
[76] W. H. Koppenol, D. M. Stanbury, P. L. Bounds, *Free Radical Biol. Med.* **2010**, *49*, 317–322.
[77] L. Wang, Q. Zhang, B. Chen, Y. Bu, Y. Chen, J. Ma, F. L. Rosario-Ortiz, R. Zhu, *Water Res.* **2020**, *174*, 115605.
[78] B. Hauchecorne, S. Lenaerts, *J. Photochem. Photobiol., C* **2013**, *14*, 72–85.
[79] H. Hussain, G. Tocci, T. Woolcot, X. Torrelles, C. Pang, D. Humphrey, C. Yim, D. Grinter, G. Cabailh, O. Bikondoa, *Nat. Mater.* **2017**, *16*, 461–466.
[80] H. Kwon, M. F. Calegari Andrade, S. Ardo, D. V. Esposito, T. A. Pham, T. Ogitsu, *ACS Appl. Mater. Interfaces* ***2024****, 16, 31687−31695.*
[81] J. Liu, H. Li, L. Zong, Q. Li, X. Wang, M. Zhang, J. Yang, *J. Nanopart. Res.* **2015**, *17*, 1–8.

[82] F. Ren, H. Li, Y. Wang, J. Yang, *Appl. Catal., B* **2015**, *176*, 160–172.
[83] X. Zeng, Y. Liu, X. Hu, X. Zhang, *Green Chem.* **2021**, *23*, 1466–1494.
[84] P. Clechet, C. Martelet, J. Martin, R. Olier, *Electrochim. Acta* **1979**, *24*, 457–461.
[85] J.-M. Herrmann, *Top. Catal.* **2005**, *34*, 49–65.
[86] J. R. Bolton, K. G. Bircher, W. Tumas, C. A. Tolman, *Pure Appl. Chem.* **2001**, *73*, 627–637.
[87] F. Amano, T. Tanaka, *Catal. Commun.* **2005**, *6*, 269–273.
[88] P. Pichat, J. M. Herrmann, J. Disdier, M. N. Mozzanega, *J. Phys. Chem.* **1979**, *83*, 3122–3126.

Manuscript received: July 12, 2024
Revised manuscript received: November 21, 2024
Accepted manuscript online: November 26, 2024
Version of record online: December 6, 2024